Fuzzy DC-Voltage Controller for a Vector Controlled Stand-Alone Induction Generator

Mateo Bašić, Dinko Vukadinović, and Miljenko Polić

Abstract— This paper presents a vector control system of the self-excited induction generator (SEIG) employing an indirect rotor-field-oriented (IRFO) control algorithm. In the system, the excitation is achieved by means of a current-controlled voltage source inverter and a single electrolytic capacitor. The objective is to keep the DC voltage across the capacitor constant and equal to the reference value, regardless of changes in the rotor speed and load. To achieve this, two different-type fuzzy logic (FL) voltage controllers are proposed and investigated. The performance of the developed FL voltage controllers is evaluated by comparison with the optimal-tuned classical PI controller. The analysis is carried out for wide ranges of rotor speed, load and DC voltage, both on the simulation and experimental level.

Keywords— Fuzzy Logic, PI Control, Self-Excited Induction Generator, Vector Control Systems.

I. INTRODUCTION

THE capability of the squirrel-cage induction generator to excite without an external reactive power source was discovered in the 1930s [1], [2]. This capability allowed the application of squirrel-cage induction generators in stand-alone power generating systems, in which the reactive power from the grid is not available. Such applications are usually associated with exploitation of renewable energy sources, especially wind energy [3]-[6]. Self-excited induction generators (SEIGs) have many advantages over other types of electric generators such as brushless construction, reduced size and cost per kW, absence of DC power supply for excitation, self-protection against short circuits, etc. Until recently, however, the widespread application of SEIGs was not possible due to the problems related with the instability of the generated voltage. Only with the advent of insulated-gate bipolar transistors (IGBTs) and microcontrollers these problems could be successfully overcome.

Mateo Bašić is with the Department of Power Engineering, Faculty of Electrical Engineering, Mechanical Engineering and Naval Architecture, University of Split, Ruđera Boškovića 32, 21000 Split, Croatia, (phone: +38521305615; fax: +38521305776; e-mail: mabasic@fesb.hr).

Dinko Vukadinović is with the Department of Power Engineering, Faculty of Electrical Engineering, Mechanical Engineering and Naval Architecture, University of Split, Ruđera Boškovića 32, 21000 Split, Croatia, (e-mail: dvukad@fesb.hr).

Miljenko Polić is with the Department of Power Engineering, Faculty of Electrical Engineering, Mechanical Engineering and Naval Architecture, University of Split, Ruđera Boškovića 32, 21000 Split, Croatia, (e-mail: miljenko.polic21@gmail.com).

Vector control algorithms, despite being more complex than the scalar counterpart, are today dominantly applied in SEIG power generating systems, largely because of their superior dynamic control features. Most of such systems reported in literature employ classical PI controllers [6]-[9] because of the inherent simple design and satisfactory control features. However, more advanced solutions based on fuzzy logic or artificial neural networks have also been considered, but those are usually adopted for efficiency optimization [5], [10], whereas when it comes to voltage and/or flux control, the classical PI controller is predominantly used. The classical PI controllers are fairly easy to implement and often can provide satisfactory performance in the operating range of interest. However, it can be argued that more sophisticated solutions, such is the one considered in this paper, should not be dismissed solely because of the greater complexity, either computational or design, especially if the difference in complexity is not that substantial while it can bring considerable improvements in performance. Besides, these advanced controllers have certain advantages over the conventional controllers. Fuzzy logic (FL) controllers, e.g., unlike the classical PI controllers, do not require knowledge of a detailed mathematical model of the control system. Furthermore, they allow a more intuitive approach to design which is due to being based on qualitative relations used in everyday language. This, in turn, makes the corresponding mathematical concepts rather easy to understand. Also, the FL controllers have the capability of handling uncertain and noisy signals, and usually lead to better results compared to the conventional controllers, in terms of response time, settling time and robustness [11]. On the down side, these improvements are usually achieved at the expense of an increase in the computational requirements. Also, designing of the FL controller can often be a complex task because it requires expert knowledge of the control system. When selecting a controller for a specific application there is one other thing to keep in mind and that is whether the use of a particular controller may jeopardize the electrical equipment and/or personnel. Therefore, the decision about which type of controller can be considered the best for a specific application is rarely an easy or straightforward decision since it requires various different aspects to be assessed.

In this paper, two different-type FL voltage controllers are proposed and developed. Their application in the SEIG vector control system is investigated and overall performance

evaluated by comparison with the optimal-tuned classical PI controller. A similar research was already conducted in [12], both on the simulation and experimental level, but it covered very limited ranges of rotor speed, load and DC voltage. In order to reach any relevant conclusions about which type of controller is better for the considered application, it is necessary to extend these ranges. Therefore, in this paper, an extensive simulation and experimental analysis is carried out for wide ranges of rotor speed, load and DC voltage. Moreover, the case when the rotor speed changes over time is also considered as it can be encountered in SEIG systems employing a variable-speed prime mover (e.g., variable-speed hydro or wind turbine).

II. SEIG VECTOR CONTROL SYSTEM

Basic configuration of the proposed vector control system is shown in Fig. 1. An indirect rotor-field-oriented (IRFO) algorithm is adopted for control of the generated voltage, as discussed in Section II *B*. The main components of the system are the induction generator, the prime mover, the IGBT converter, the IRFO controller and the DC link. The battery in the DC link provides the initial voltage across the capacitor *C* for initial excitation of the induction generator. As soon as the voltage across the capacitor rises to a value higher than the battery voltage, the battery is automatically switched off through diode. The resistive load R_{dc} is connected in parallel with the capacitor. The main control objective is to ensure that the voltage across the capacitor remains constant and equal to the reference value, regardless of changes in the rotor speed and load. This is achieved by adjusting the active and reactive power flow in the system through control of the IGBT converter switching pulses. These pulses are generated at the output of the hysteresis current controllers, as shown in Fig. 4, with the reference phase currents calculated within the IRFO control algorithm. In the proposed control system, measurement of the following variables is required: the rotor speed, the DC-link voltage and the phase currents (all three or just two – in the case of isolated stator neutral). As for the prime mover, the following two cases are investigated in this paper: fixed-speed prime mover and variable-speed prime mover.
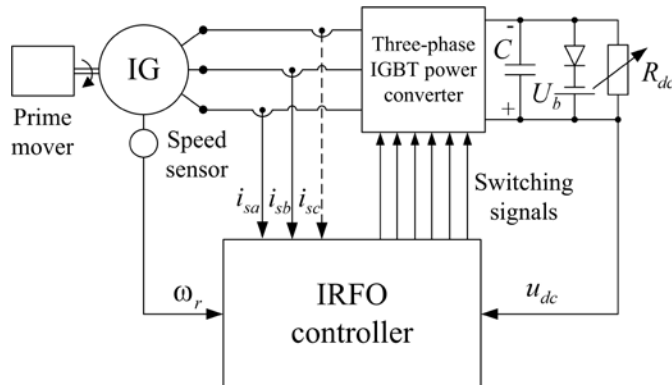

Fig. 1 Basic configuration of the SEIG vector control system

A. Modeling of the Control System Components

In general, application of the vector control algorithm requires a dynamic SEIG model to be defined. Such model can be obtained by modification of the conventional dynamic model of an induction machine, as described in [13]. The conventional dynamic SEIG model, expressed in the Laplace domain and suitable for use in MATLAB Simulink, is described in the stationary reference frame by the following 1st order differential equations:

$$si_{s\alpha} = \frac{1}{\sigma L_s L_r}(L_m^2 \omega_r i_{s\beta} - L_r R_s i_{s\alpha} + L_m \omega_r L_r i_{r\beta} + \\ + L_m R_r i_{r\alpha} - L_r u_{s\alpha} - L_m K_{r\alpha}) \tag{1}$$

$$si_{s\beta} = \frac{1}{\sigma L_s L_r}(-L_r R_s i_{s\beta} - L_m^2 \omega_r i_{s\alpha} + L_m R_r i_{r\beta} - \\ - L_m \omega_r L_r i_{r\alpha} - L_r u_{s\beta} - L_m K_{r\beta}) \tag{2}$$

$$si_{r\alpha} = \frac{1}{\sigma L_s L_r}(L_m R_s i_{s\alpha} - L_s \omega_r L_m i_{s\beta} - L_s \omega_r L_r i_{r\beta} - \\ - L_s R_r i_{r\alpha} + L_m u_{s\alpha} - L_s K_{r\alpha}) \tag{3}$$

$$si_{r\beta} = \frac{1}{\sigma L_s L_r}(L_m R_s i_{s\beta} + L_s \omega_r L_m i_{s\alpha} - L_s R_r i_{r\beta} + \\ + L_s \omega_r L_r i_{r\alpha} + L_m u_{s\beta} - L_s K_{r\beta}) \tag{4}$$

where:

$u_{s\alpha}$ and $u_{s\beta}$ are the α-axis and β-axis component of the stator phase voltage space-vector;

$i_{s\alpha}$ and $i_{s\beta}$ are the α-axis and β-axis component of the stator phase current space-vector;

$i_{r\alpha}$ and $i_{r\beta}$ are the α-axis and β-axis component of the rotor phase current space-vector;

R_s and R_r are the stator and rotor resistance, respectively;

L_s, L_r and L_m are the stator inductance, the rotor inductance and the magnetizing inductance, respectively;

ω_r is the rotor angular speed;

σ is the total leakage factor;

$K_{r\alpha}$ and $K_{r\beta}$ are the α-axis and β-axis component of the voltage initially induced due to the residual rotor flux linkage.

Fig. 2 shows the conventional SEIG equivalent circuit described by (1)-(4). Only the equivalent circuit for the α-axis is shown since all the physical phenomena along the β-axis are analogous, with a phase shift of 90° el.

Saturation of the magnetizing flux is taken into account by expressing the magnetizing inductance as a function of the magnetizing current magnitude. It is, in fact, mandatory for build-up and stabilization of the SEIG's generated voltage to be possible. The magnetizing characteristic of the considered induction machine (parameters given in Appendix) was determined from the standard no-load test, as described in [13], [14]. The characteristic is shown in Fig. 3.
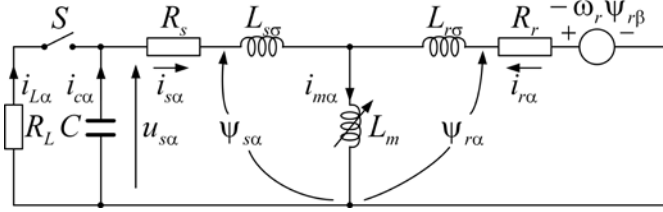
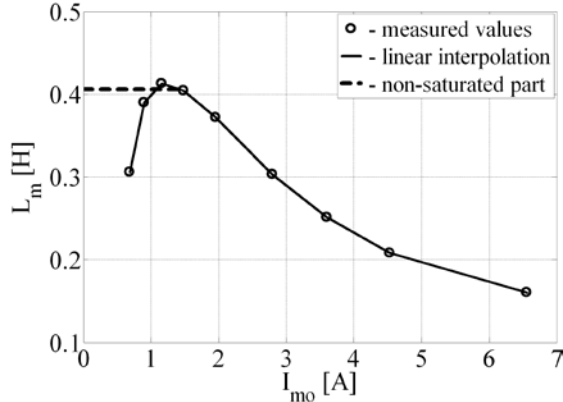Fig. 2 Conventional SEIG equivalent circuit in stationary reference frame (α-axis)

Fig. 3 No-load magnetizing characteristic

The steady-state operating point of a SEIG is always positioned somewhere in the saturated part of the characteristic, i.e., right of the peak. The non-saturated part is usually represented by a fixed value of the magnetizing inductance (dashed line in Fig. 3).

Note that, for convenience, the iron losses of the SEIG are neglected. This is well justified by the fact that the investigation in this paper is not focused on the system's efficiency or detuning-related phenomena, but rather on determining the appropriate DC-voltage controller.

The SEIG model shown in Fig. 2 is applicable in cases where the parallel combination of the capacitor and resistive load is connected directly to the induction machine's stator terminals. However, in the system shown in Fig. 1, there is one additional component placed between the stator terminals and the DC link, which is the IGBT converter, so the corresponding model also needs to be determined and fitted into the system's equations.

By assuming ideal three-phase IGBT converter, the stator phase voltages and the DC-link current can be expressed in terms of the converter's switching functions as

$$u_{sa} = \frac{1}{3} u_{dc} \left(2 S_a - S_b - S_c \right) \tag{5}$$

$$u_{sb} = \frac{1}{3} u_{dc} \left(2 S_b - S_c - S_a \right) \tag{6}$$

$$u_{sc} = \frac{1}{3} u_{dc} \left(2 S_c - S_a - S_b \right) \tag{7}$$

$$i_{dc} = S_a i_{sa} + S_b i_{sb} + S_c i_{sc} \tag{8}$$

where u_{dc} is the voltage across the DC-link capacitor, and i_{sa}, i_{sb} and i_{sc} are the stator phase currents. Values of the switching functions S_a, S_b and S_c are generated at the output of the hysteresis current controller in the given phase.

The DC link can be described by the following equation:

$$u_{dc} = -\frac{1}{C} \int_0^t \left(i_{dc} + \frac{u_{dc}}{R_{dc}} \right) dt + u_{dc0} \tag{9}$$

where C is the DC-link capacitor, R_{dc} is the DC-link resistive load and u_{dc0} is the battery voltage.

B. Control Algorithm

The proposed IRFO control algorithm is shown in Fig. 4. It allows the SEIG magnetization level and torque to be separately controlled and adjusted by controlling the mutually perpendicular components of the stator phase current space-vector along the d and q axes. The reference d-axis component of the stator phase current space-vector is therefore responsible for magnetization, whereas the corresponding q-axis component (hereinafter: reference q-axis stator current) is responsible for torque adjustment. The reference rotor flux linkage is calculated online as proportional to the ratio of the reference DC voltage u_{dc}^* and measured rotor speed ω_r, with the proportionality factor k_ψ.
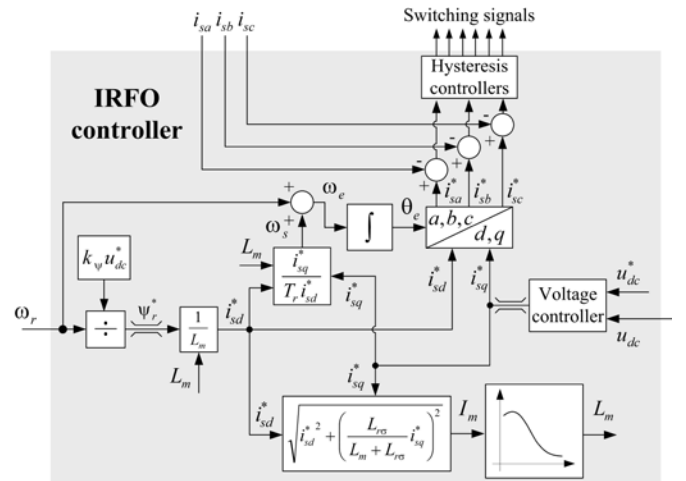

Fig. 4 IRFO controller schematic diagram

The reference and the actual DC voltage represent the input variables for the DC-voltage controller, whereas the reference q-axis stator current represents the output variable. However, the relationship between the input and output variables is not yet defined since the appropriate DC-voltage controller has yet to be determined. This issue is addressed in the next section, where the classical PI controller and two different-type FL controllers are considered as possible solutions.

III.   DC-VOLTAGE CONTROLLERS

A.   Classical PI Voltage Controller

The classical PI controller can be described by

$$y(t) = K_P \varepsilon(t) + \frac{K_P}{T_I} \int_0^t \varepsilon(t)dt \qquad (10)$$

where $\varepsilon(t)$ is the input error signal and $y(t)$ is the output control signal. In this case: $\varepsilon(t) = u_{dc}^*(t) - u_{dc}(t)$ and $y(t) = i_{sq}^*(t)$. The PI controller's operating principle can be summarized as follows: the value of the output signal $y(t)$ is exactly such that it allows the input error signal $\varepsilon(t)$ to be reduced to zero (due to integral part). K_P and T_I denote the proportional gain and the integral time constant of the PI controller, respectively. These parameters can be set to optimal values by observing the PI controller's response to step changes in the reference value and disturbances in the system (e.g., abrupt changes in load). Such approach was adopted in Section IV A.

B.   FL Voltage Controllers

In this paper, two different-type FL voltage controllers, i.e., Mamdani-type and Sugeno-type, are developed. Generally, Mamdani-type controllers allow a more intuitive approach to design and are more widely accepted, whereas Sugeno-type controllers are computationally more efficient, which can prove to be a great advantage when it comes to real-time application. Both FL controllers developed in this paper have the same number of inputs (2), outputs (1) and fuzzy rules (25). Fig. 5 shows the membership functions (MFs) of the Mamdani-type FL controller, where N, P and Z stand for *negative*, *positive* and *zero*, respectively, whereas S, M and B stand for *small*, *medium* and *big*, respectively. Hence, NS is interpreted as *small negative*. In Fig. 5, e is the input error signal expressed in per unit values and calculated at each sampling instant as the difference between the reference and the actual DC voltage; ce is the additional input signal, also expressed in per unit values, which contains the information about the rate of change of the error; $cisq$ is the output per-unit signal utilized for adjustment of the reference q-axis stator current. The output signal is calculated at each sampling instant and added to the previous value so, by accumulation, the actual value of the reference q-axis stator current is obtained. In this paper, the scaling factors of 0.005, 0.4 and 0.1 were adopted for e, ce and $cisq$, respectively.

The input MFs of the Sugeno-type FL controller match those of the Mamdani-type, however the output MFs are quite different. Namely, as opposed to the triangular-shaped output MFs of the Mamdani-type FL controller, the Sugeno-type FL controller utilizes singleton output MFs of the following values: NB = -2, NM = -1, NS = -0.5, Z = 0, PS = 0.5, PM = 1 and PB = 2. This, in effect, allows higher computational efficiency compared to the Mamdani-type FL controller, which is beneficial from the viewpoint of real-time application.
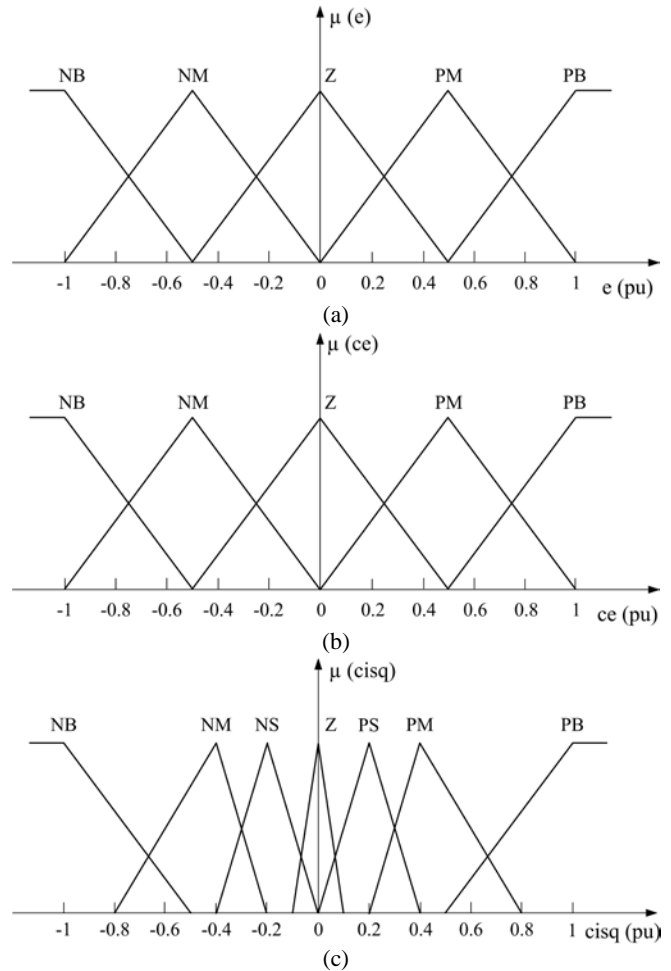

Fig. 5 Membership functions of the developed Mamdani-type FL controller: (a) input e, (b) input ce, (c) output $cisq$

The centroid defuzzification method was utilized for the Mamdani-type FL controller, whereas the weighted average defuzzification method was utilized for the Sugeno-type FL controller. These are, actually, default defuzzification methods in the FIS Editor (MATLAB) offered for these two types of FL controllers. Furthermore, the operation of the FL controllers is governed by the set of IF-THEN rules summarized in Table 1. Of course, only four of them are active at the same time. The same set of rules applies to both developed FL controllers, where a typical rule reads: 'IF e is NM AND ce is PM THEN $cisq$ is Z'. Also, for both developed FL controllers, the degree of membership of AND(e, ce) is defined by *minimum*.

Table 1 Rule base for FL controllers

e \ ce	NB	NM	Z	PM	PB
NB	PB	PB	PM	PS	Z
NM	PB	PM	PS	Z	NS
Z	PM	PS	Z	NS	NM
PM	PS	Z	NS	NM	NB
PB	Z	NS	NM	NB	NB

IV. SIMULATION RESULTS

The simulation model of the proposed SEIG control system was built in the MATLAB Simulink environment. Within the simulation model, two different sampling times were used: the sampling time T_{s1} = 1/28000 s was used for the induction generator, the IGBT converter and the hysteresis current controllers, whereas the sampling time T_{s2} = 1/4000 s was used for the rest of the model. In this way, several important goals were achieved without compromising the performance of the control algorithm, and those are as follows: sufficiently high switching frequency for the IGBTs, sufficiently accurate numerical model of the induction machine, which primarily refers to solving the corresponding nonlinear differential equations, and, finally, reduced computational requirements.

A. Optimization of the PI Voltage Controller

In order to ensure a relevant comparison and evaluation of the PI and FL controllers' overall performances, first it was necessary to determine the optimal values for the PI controller's parameters. Therefore, the simulations were carried out for three different parameter settings shown in Table 2. The 1st parameter setting in Table 2 has the smallest T_I value, whereas the 3rd parameter setting has the largest K_P value. In that sense, the 2nd parameter setting represents an in-between option.

Table 2 PI controller parameter settings

	K_P [A/V]	T_I [s]
1st setting	0.02	0.05
2nd setting	0.02	0.1
3rd setting	0.05	0.1

The performance of three different-tuned PI controllers was analyzed for the following cases:

1. At t = 2 s, the load resistance of R_{dc} = 500 Ω is applied, whereas both the rotor speed and reference DC voltage are kept constant and equal to 1200 rpm and 300 V, respectively (Fig. 6).

2. At t = 2 s, the reference DC voltage is changed in a step manner from u_{dc}^* = 250 V to u_{dc}^* = 300 V, whereas both the rotor speed and load resistance are kept constant and equal to 1200 rpm and 220 Ω, respectively (Fig. 7).

According to Fig. 6a, the 3rd parameter setting from Table 2 ensures fast response combined with the lowest DC voltage drop compared to the other two parameter settings. Furthermore, when the criteria of lowest overshoot/undershoot, and shortest settling time are applied to the responses shown in Figs. 6b and 7a, again the same parameter setting seems to provide the best results. However, in Fig. 7b it can be observed that the 3rd parameter setting is associated with the poorest transient behavior of the reference q-axis stator current for the case of a step change in the reference DC voltage. Namely, the reference q-axis stator current and, consequently, the stator phase currents have the highest peak value when the

PI controller is tuned according to the 3rd parameter setting. This is due to the largest K_P value since it results in the largest change in the output for a given change in the error. In this case, the peak value of the q-axis stator current obtained for the 3rd parameter setting is exactly 2.5 times higher compared to the other two parameter settings, which is exactly the ratio of the corresponding proportional gains (i.e., 0.005/0.002).

As for the 1st and 2nd parameter settings from Table 2, the 1st parameter setting seems to offer faster responses compared to the 2nd parameter setting according to the results shown in Figs. 6 and 7a, which is due to the smaller integral time constant. However, the faster responses are achieved at the expense of an increase in oscillations in Fig. 6a and overshoot/undershoot values in Figs. 6b and 7a (about 7 % higher). Moreover, in Fig. 7a, the voltage overshoot obtained for the 1st parameter setting exceeds 10 %, whereas the settling time is 0.127 s longer compared to that obtained for the 2nd parameter setting. In Fig. 7b, the same peak value of the reference q-axis stator current was noted for these two parameter settings, which is due to the same proportional gain. However, the faster response was in this case noted for the 2nd parameter setting.

Based on the presented results, ultimately it can be said that both the 1st and 3rd parameter settings do not provide satisfactory overall results. In the case of the 1st parameter setting, it is due to too small integral time constant, whereas in the case of the 3rd parameter setting, it is due to too large proportional gain. Therefore, the 2nd parameter setting seems to stand out as the best choice since it incorporates the requirements of the fast response, low overshoots/undershoots and safety.
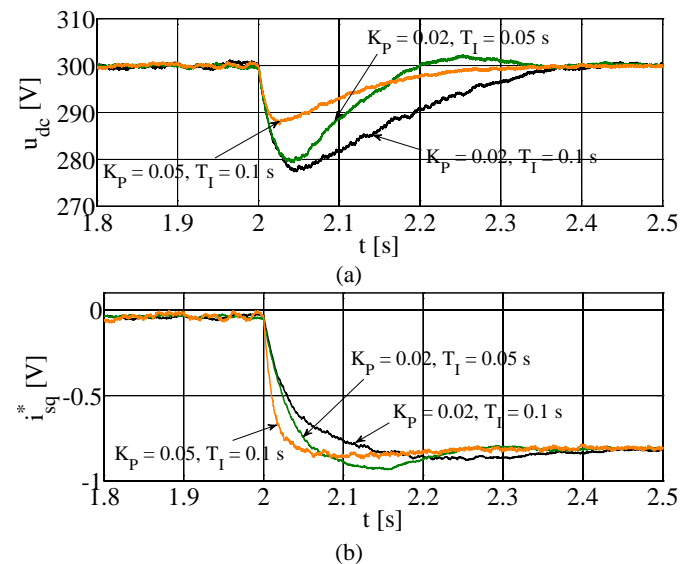

Fig. 6 Simulation responses to step change in load for different-tuned PI controllers: (a) actual DC voltage, (b) q-axis stator current reference
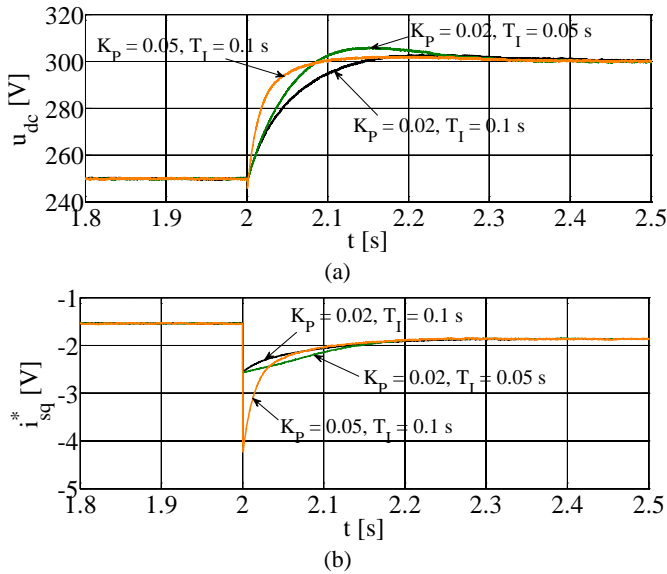
Fig. 7 Simulation responses to step change in reference DC voltage for different-tuned PI controllers: (a) actual DC voltage, (b) q-axis stator current reference

Before moving on to comparison of the PI and FL voltage controllers, there is one other thing to keep in mind: in the case of the PI controller, a step change in the reference DC voltage always results in rather abrupt and steep change in the q-axis stator current, regardless of the parameter setting (Fig. 7b); this, in turn, can lead to dangerously high voltages induced in the stator phase windings and overheating of the electric machinery/equipment, which can potentially cause irreversible damage to the stator windings' insulation. Increasing the step value and/or the proportional gain would lead to even higher peak currents and induced voltages. This issue cannot be solved by limiting the output value of the PI controller. On the contrary, that kind of approach could lead to other problems – saturation of the PI controller's integrator, followed by a loss of control of the DC voltage and, eventually, complete demagnetization of the SEIG.

B. Comparison of the PI and FL Voltage Controllers

In this section, the performance of the developed FL controllers is evaluated and compared with that of the optimal-tuned classical PI controller.

In the first set of simulations, the load resistance is varied in a step manner as shown in Table 3. The following two cases are considered: fixed rotor speed and variable rotor speed.

Table 3 Step changes in load resistance

t [s]	$0 - 2$	$2 - 5$	$5 - 8$	$8 - 10$
R_{dc} [Ω]	10^{12}	500	220	500

Figs. 8 and 9 show the simulation responses of the actual DC voltage and reference q-axis stator current obtained for the fixed rotor speed of $n = 1200$ rpm and two different values of the reference DC voltage.
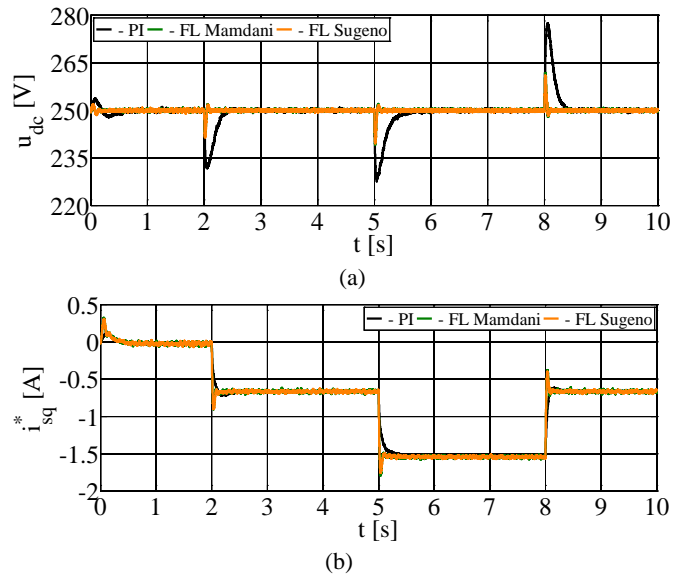

Fig. 8 Responses to step changes in load resistance ($n = 1200$ rpm, $u_{dc}^* = 250$ V): (a) actual DC voltage, (b) reference q-axis stator current
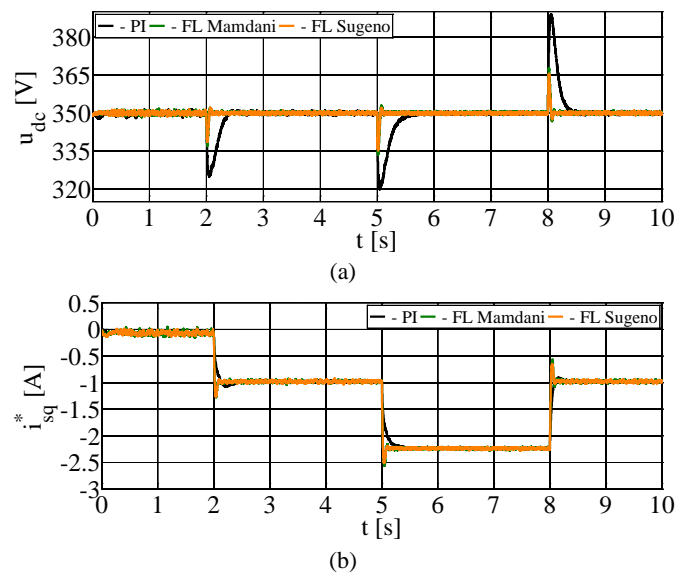

Fig. 9 Responses to step changes in load resistance ($n = 1200$ rpm, $u_{dc}^* = 350$ V): (a) actual DC voltage, (b) reference q-axis stator current

For the case of fixed rotor speed, similar responses to load disturbance are obtained for both considered values of the reference DC voltage. Also, in both cases, the FL controllers provide about four times faster responses of the actual DC voltage compared to the optimal-tuned PI controller, with about twice as low voltage drop/rise values. The FL controllers provide faster response of the reference q-axis stator current as well, with about 0.2 s shorter settling time compared to the PI controller. On the down side, the overshoots/undershoots in the reference q-axis stator are about 25 % higher compared to the PI controller.

Fig. 10 shows the simulation response of the actual DC voltage obtained for the case of the sinusoidal disturbance $n_D = 200\sin(2\pi 0.5t)$ rpm imposed to the rotor speed of 1200 rpm, i.e., $n = 1200$ rpm + n_D. The reference DC voltage is equal to 300 V.

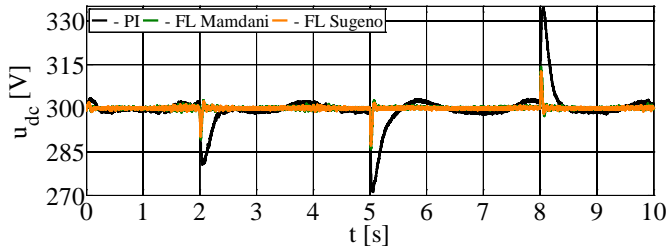Fig. 10 Actual DC voltage response to step changes in load resistance ($n = 1200 + 200\sin(2\pi 0.5t)$ rpm, $u_{dc}^* = 300$ V)

As it can be observed, the FL controllers exhibit more robust response to the speed disturbance compared to the PI controller. In fact, the results obtained for the FL controllers in this case pretty much resemble those obtained in the case of fixed rotor speed. On the other hand, notable oscillations appear in the DC voltage in the case when the PI controller is used. It can be argued that the sinusoidal speed disturbance of frequency 0.5 Hz and amplitude 200 rpm, such is imposed here, is not likely to be encountered in real SEIG systems, especially given the dynamics of commonly used prime movers (e.g., variable-speed hydro or wind turbines). However, the speed disturbance was intentionally exaggerated to show the superiority of the developed FL controllers over the classical PI controller in terms of robustness to speed disturbances in general. Of course, various speed disturbances do occur in real SEIG systems (e.g., disturbances related to stochastic wind variations or water flow dynamics), whereas the task of the voltage controller, among other things, is to successfully deal with them. In defense of the PI controller, it should be said that in the case of a less severe speed disturbance with five times lower frequency, which was also considered in the investigation, the PI controller exhibited satisfactory performance, as with fixed rotor speed.

In the second set of simulations, the reference DC voltage is varied in a step manner as shown in Table 4. Again, the cases with fixed and variable rotor speed are considered.

Table 4 Step changes in reference DC voltage

t [s]	0 – 2	2 – 4	4 – 6
u_{dc}^* [V]	250	300	250

Figs. 11 and 12 show the simulation responses of the actual DC voltage and reference q-axis stator current obtained for the fixed rotor speed of $n = 1200$ rpm and two different values of the load resistance.
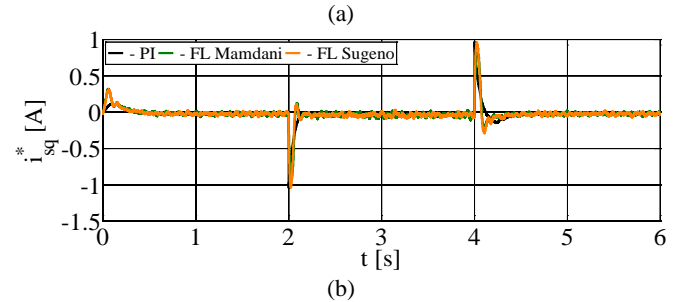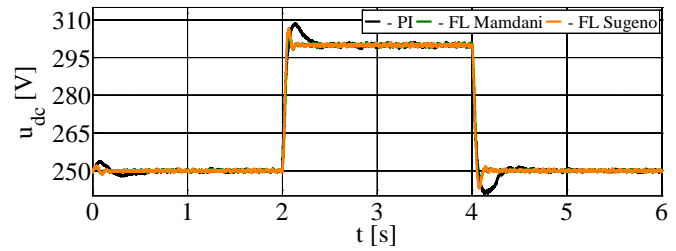

(a)

(b)

Fig. 11 Responses to step changes in reference DC voltage ($n = 1200$ rpm, $R_{dc} = 10^{12}$ Ω): a) actual DC voltage, b) reference q-axis stator current

(a)

(b)

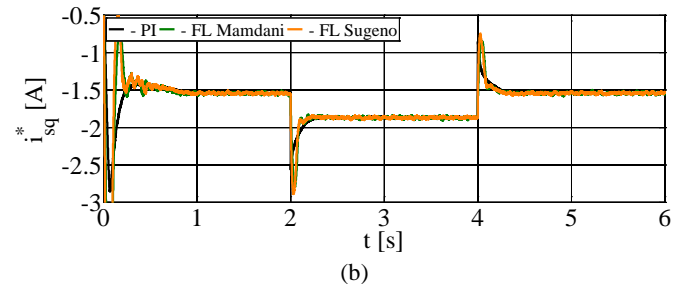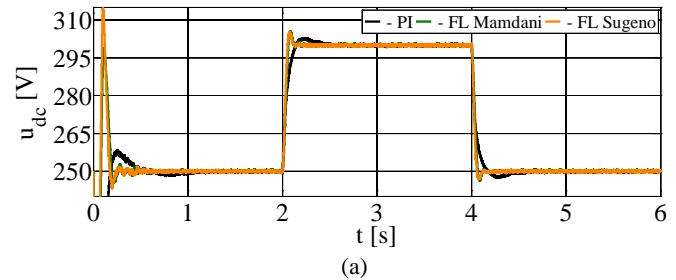Fig. 12 Responses to step changes in reference DC voltage ($n = 1200$ rpm, $R_{dc} = 220$ Ω): a) actual DC voltage, b) reference q-axis stator current

Compared to the PI controller, the FL controllers ensure notably faster response of the actual DC voltage to step changes in the reference value, in terms of rise and settling times, while retaining approximately the same and in some cases even lower overshoot/undershoot values. As for the peak values of the reference q-axis stator current, at no load, there is no significant difference regardless of the controller used, whereas for the connected load, the peaks obtained for the FL controllers are up to 12.5 % higher compared to the PI controller. However, this is to some extent compensated by a less steep change in the reference q-axis stator current (i.e., lower derivation).

Fig. 13 shows the simulation response of the actual DC voltage obtained for the case of the sinusoidal disturbance of $n_D = 200\sin(2\pi 0.5t)$ rpm imposed to the rotor speed of 1200 rpm, i.e., $n = 1200$ rpm $+ n_D$. The load resistance of $R_{dc} = 220$ Ω is applied.
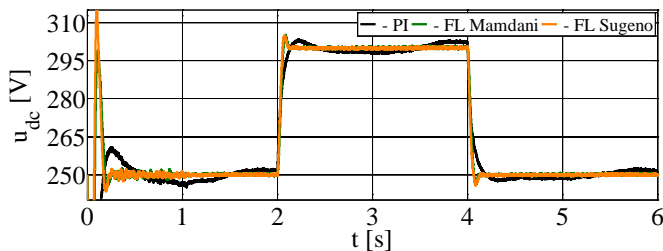

Fig. 13 Actual DC voltage response to step changes in reference DC voltage ($n = 1200 + 200\sin(2\pi 0.5t)$ rpm, $R_{dc} = 220$ Ω)

The results confirm greater robustness of the FL controllers to speed disturbances, although it has to be said that the PI controller's robustness to such speed disturbance increases with decreasing load. For example, at no load, there is no much difference between the responses obtained with fixed and variable rotor speed.

The simulation results presented in this section suggest that the developed FL controllers exhibit better overall performance compared to the PI controller. In addition to that, the responses obtained for the Mamdani-type and Sugeno-type FL controllers are almost overlapping, indicating quite similar performance in terms of voltage control. According to the criterion of computational efficiency, however, the Sugeno-type FL controller clearly stands out as a better choice. This is confirmed by the fact that the corresponding simulation execution times were about 9 % shorter compared to the Mamdani-type FL controller. Further shortening of the simulation execution times is achieved by converting the Sugeno-type FL controller, originally developed in the FIS Editor, into C code. Consequently, the simulation execution times with the Sugeno-type FL controller came to be only 2 % longer compared to those with the PI controller, while the exact control features of the originally developed controller were retained (i.e., overlapping responses). Therefore, it was decided that only the classical PI controller and the Sugeno-type FL controller written in C code are to be used for the experimental analysis.

V. EXPERIMENTAL RESULTS

For experimental validation of the simulation results, the experimental setup of the SEIG control system under consideration was built (Fig. 14). The IRFO control algorithm was programed in MATLAB Simulink and executed in real time by using the DS1104 R&D Controller Board, manufactured by dSpace.
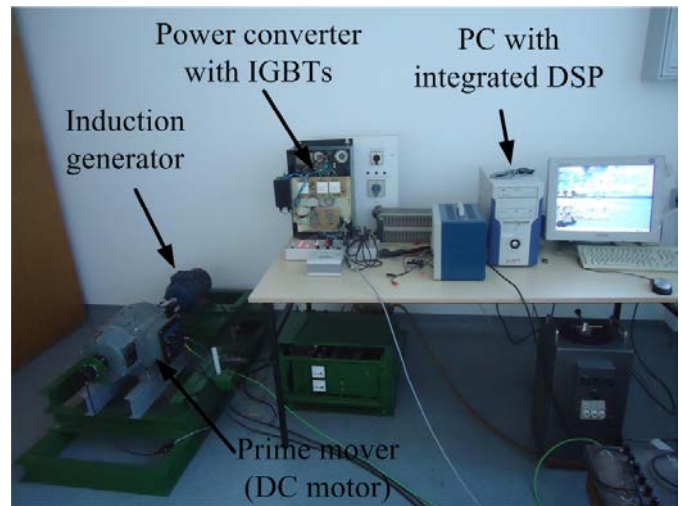

Fig. 14 SEIG control system experimental setup

The operating regimes considered in the first set of experiments are the same as those described in Section IV *B* for the case of step changes in the load resistance, only in this case the load resistance was varied manually so the related transients did not occur at exactly the same times as in the simulations, but rather at approximate times. For the same reason, there is also a slight time offset between the experimental responses obtained for the PI and the FL controller. However, the analysis itself is in no way affected by this.

The experimental results in Figs. 15 and 16 are equivalent to the simulation results in Figs. 8 and 9. As it can be seen, the experimental results are in good agreement with the simulation results, thus the previous conclusions are hereby confirmed.
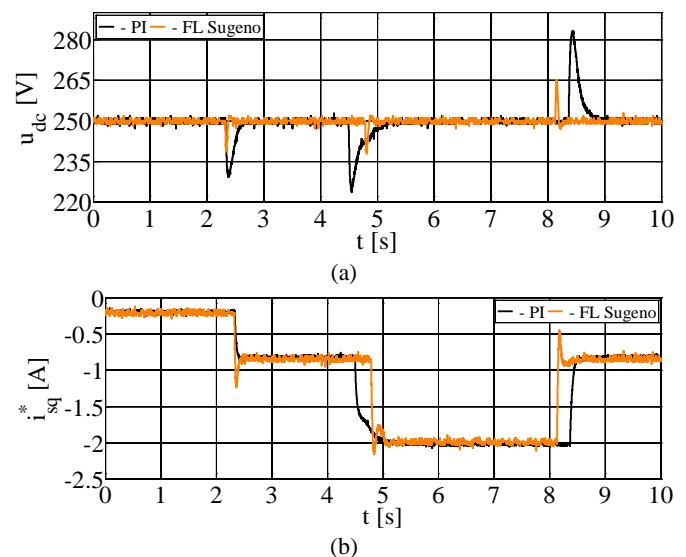

(a)

(b)

Fig. 15 Responses to step changes in load resistance ($n = 1200$ rpm, $u_{dc}^* = 250$ V): (a) actual DC voltage, (b) reference *q*-axis stator current
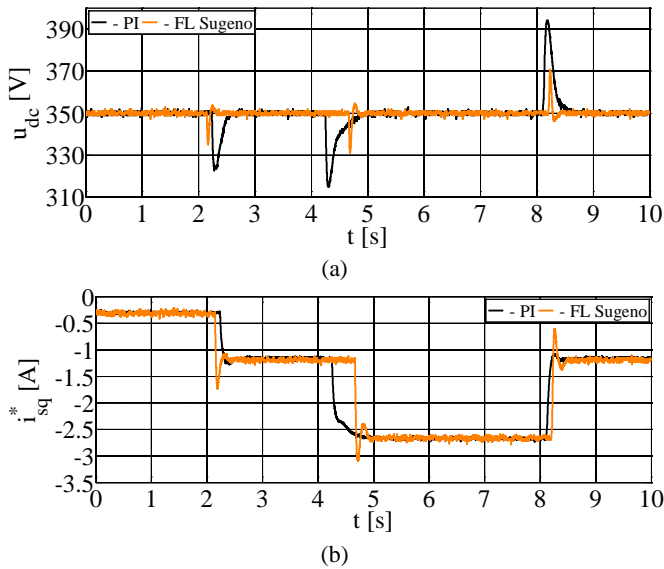
(a)

(b)

Fig. 16 Responses to step changes in load resistance (n = 1200 rpm, u_{dc}^* = 350 V): (a) actual DC voltage, (b) reference q-axis stator current

The largest disagreement between the experimental and simulation results is noted in the steady-state values of the reference q-axis stator current. This is due to the fact that certain losses which exist in the real SEIG system are not accounted for in the simulation model (e.g., the power converter losses and the induction machine mechanical, iron and stray losses). Omitting these additional losses results in lower torque values obtained in the simulations and, consequently, in lower steady-state values of the reference q-axis stator current (reference d-axis stator current is of the same value). Nevertheless, the analysis of the power losses and related phenomena is beyond the scope of this paper since these do not depend on the type of the voltage controller used.

The experimental results in Fig. 17 are equivalent to the simulation results in Fig. 10. As in the simulations, the FL controller exhibits more robust response to the imposed speed disturbance compared to the PI controller.
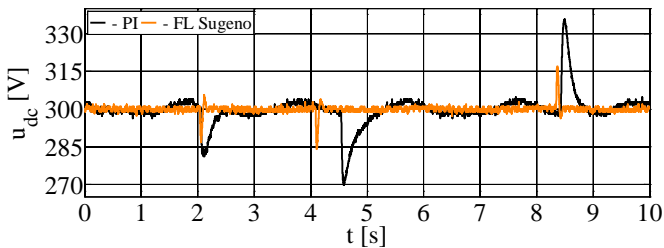

Fig. 17 Actual DC voltage response to step changes in load resistance (n = 1200 + 200sin(2π0.5t) rpm, u_{dc}^* = 300 V)

The operating regimes considered in the second set of experiments are the same as those described in Section IV *B* for the case of step changes in the reference DC voltage. For the already explained reasons, a time offset appeared between the experimental and simulation responses as well as between the experimental responses obtained for the two controllers.

Figs. 18 and 19 show the experimental results which are equivalent to the simulation results in Figs. 11 and 12. Again, the FL controller exhibits significantly faster response compared to the PI controller, but the price was paid in higher overshoots/undershoots in the actual DC voltage (up to 14 % higher), as well as in higher peak values of the reference q-axis stator current (up to 34 % higher), especially in the case when the load is connected. The experimental overshoots/undershoots are slightly higher than those noted in the simulations, regardless of the type of controller, which is again due to existence of the additional losses not accounted for in the simulation model. As in the simulations, the PI controller exhibits rather abrupt response to a step change in the reference DC voltage.
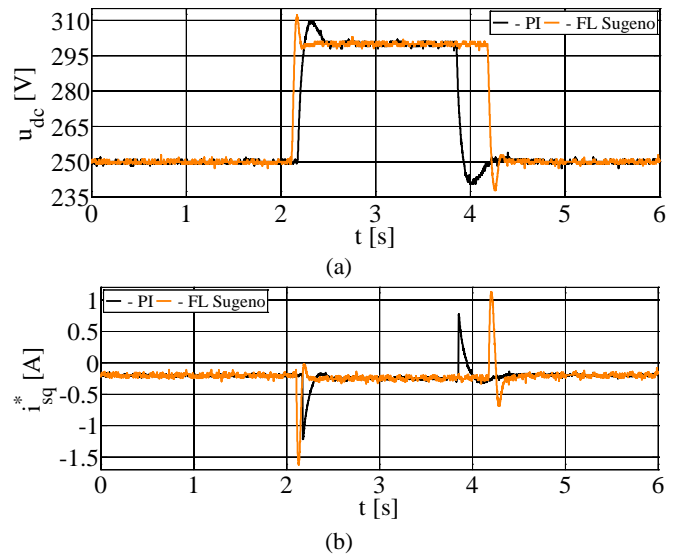

(a)

(b)

Fig. 18 Responses to step changes in reference DC voltage (n = 1200 rpm, R_{dc} = 10^{12} Ω): (a) actual DC voltage, (b) reference q-axis stator current

(a)
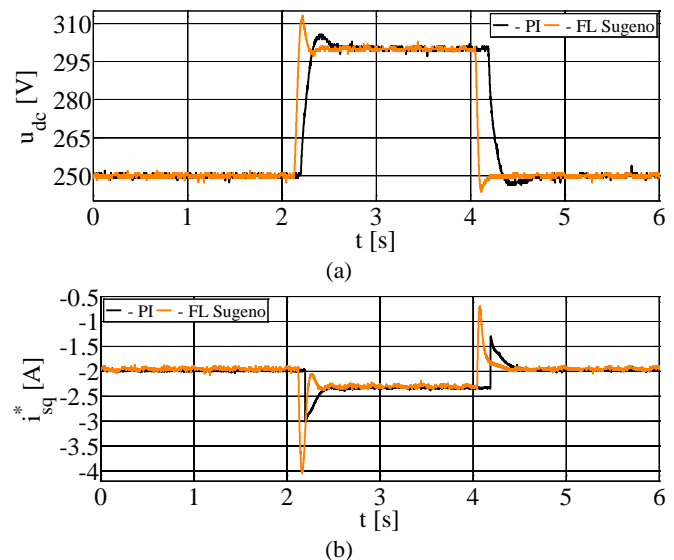

(b)

Fig. 19 Responses to step changes in reference DC voltage (n = 1200 rpm, R_{dc} = 220 Ω): (a) actual DC voltage, (b) reference q-axis stator current

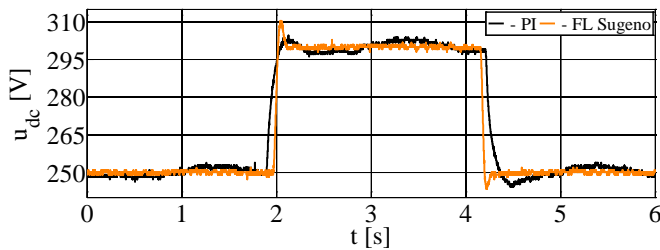Finally, the experimental results in Fig. 20 are equivalent to the simulation results in Fig. 13.

Fig. 20 Actual DC voltage response to step changes in reference DC voltage ($n = 1200 + 200\sin(2\pi 0.5t)$ rpm, $R_{dc} = 220\ \Omega$)

It can be observed that the FL controller provides much more stable DC voltage compared to the PI controller.

VI. CONCLUSION

In this paper, the performance of the proposed FL controllers was investigated and evaluated by comparison with the optimal-tuned classical PI controller. The analysis encompassed rather wide ranges of rotor speed, DC voltage and load. The simulation results showed that the two developed FL controllers offer quite similar performance in terms of overshoot/undershoot, response time, settling time and robustness. By the same criteria, their overall performance was evaluated better compared to the optimal-tuned PI controller. However, the improvement in performance was achieved at the expense of an increase in the computational requirements, especially in the case of the Mamdani-type FL controller. Hence, only the Sugeno-type FL controller, being the computationally more efficient one, was used in the experimental analysis. The computational efficiency of the Sugeno-type FL controller was further increased by conversion to C code. Good agreement was achieved between the experimental and simulation results. In fact, the largest disagreement was noted in the steady-state values of the reference q-axis stator current, which is due to the additional losses not accounted for in the simulation model, and has nothing to do with the type of controller used. The increase of the phase currents' peak values obtained for the proposed FL controllers can be considered as their biggest disadvantage compared to the optimal-tuned classical PI controller. Still, this drawback is at least compensated if not surpassed by other favorable features, thus proving the validity of the proposed FL-based approach. This is not to say that it is the best possible approach, but rather that it should be at least seriously considered as a promising alternative to conventional PI-based solutions.

APPENDIX

Induction machine parameters
P_n=1.5 kW, U_n=380 V, p=2, Y, I_n=3.81 A, n_n=1391 rpm, L_m^n=0.4058 H, $L_{s\sigma}$=0.01823 H, $L_{r\sigma}$=0.02185 H, R_s=4.293 Ω, R_r=3.866 Ω (at 20 °C), Ψ_{rn} = 0.845 Wb.

REFERENCES

[1] E. D. Basset and F. M. Potter, "Capacitive Excitation for Induction Generators", *AIEE Trans. Electrical Engineering*, vol. 54, pp. 540–545, May 1935.

[2] C. Wagner, "Self-excitation of Induction Motors", *AIEE Trans. Electrical Engineering*, vol. 58, pp. 47–51, February 1939.

[3] A. M. Kassem, "Predictive Voltage Control of Stand Alone Wind Energy Conversion System", *WSEAS Trans. Systems and Control*, vol. 7, pp. 97–107, July 2012.

[4] K.S. Sandhu and S.P.Jain, "Steady State Operation of Self-Excited Induction Generator with Varying Wind Speeds", *International Journal of Circuits, Systems and Signal Processing*, vol. 2, pp. 26–33, 2008.

[5] R. M. Hilloowala and A. M. Sharaf, "A Rule-Based Fuzzy Logic Controller for a PWM Inverter in a Stand Alone Wind Energy Conversion Scheme", *IEEE Trans. Industry Applications*, vol. 32, pp. 57–65, January/February 1996.

[6] K. Idjdarene, D. Rekioua, T. Rekioua, and A. Tounzi, "Vector Control of Autonomous Induction Generator Taking Saturation Effect Into Account", *Energy Conversion and Management*, vol. 49, pp. 2609–2617, October 2008.

[7] E. Margato, J. Faria, M. J. Resende, and J. Palma, "A New Control Strategy with Saturation Effect Compensation for an Autonomous Induction Generator Driven by Wide Speed Range Turbines", *Energy Conversion and Management*, vol. 52, pp. 2142–2152, May 2011.

[8] Y. W. Liao and E. Levi, "Modelling and Simulation of a Stand-Alone Induction Generator with Rotor Flux Oriented Control", *Electric Power Systems Research*, vol.46, pp. 141–153, June 1998.

[9] R. Leidhold, G. Garcia, and M. I. Valla, "Field-Oriented Controlled Induction Generator with Loss Minimization", *IEEE Trans. Industrial Electronics*, vol. 49, pp. 147–156, February 2002.

[10] D. Vukadinović and M. Bašić, "A Stand-Alone Induction Generator with Improved Stator Flux Oriented Control", *Journal of Electrical Engineering*, vol. 62, pp. 65–72, 2011.

[11] J. M. Zurada, R. J. Marks, and C. J. Robinson, *Computational Intelligence Imitating Life*. Piscataway, NJ: IEEE Press, 1994.

[12] M. Bašić, D. Vukadinović, and M. Polić, "Fuzzy Logic vs. Classical PI Voltage Controller for a Self-Excited Induction Generator", in *Proc. 4th Eur. Conf. AMATHI*, Dubrovnik, 2013, pp. 189-194.

[13] M. Bašić, D. Vukadinović, and G. Petrović, "Dynamic and Pole-Zero Analysis of Self-Excited Induction Generator Using a Novel Model with Iron Losses", *International Journal of Electrical Power & Energy Systems*, vol. 42, pp. 105–118, November 2012.

[14] M. Bašić, D. Vukadinović, and D. Lukač, "Novel dynamic model of self-excited induction generator with iron losses", *International Journal of Mathematical Models and Methods in Applied Sciences*, vol. 5, pp. 221–229, 2011.